



Electrokinetic Energy Conversion in Nanochannels Grafted with pH-responsive Polyelectrolyte Brushes Modelled Using Augmented Strong Stretching Theory

Journal:	<i>Soft Matter</i>
Manuscript ID	SM-ART-04-2019-000765.R1
Article Type:	Paper
Date Submitted by the Author:	25-Jun-2019
Complete List of Authors:	Sachar, Harnoor; University of Maryland, College Park, Mechanical Engineering Sivasankar, Vishal; University of Maryland, College Park, Mechanical Engineering Das, Siddhartha; University of Maryland, College Park, Mechanical Engineering

Electrokinetic Energy Conversion in Nanochannels Grafted with pH-responsive Polyelectrolyte Brushes Modelled Using Augmented Strong Stretching Theory

Harnoor Singh Sachar, Vishal Sankar Sivasankar, and Siddhartha Das

Department of Mechanical Engineering, University of Maryland, College Park, MD-20742, USA

(Dated: June 25, 2019)

Abstract:

In this paper, we develop a theory to quantify the electrokinetic energy conversion in electrolyte-filled nanochannels grafted with pH-responsive polyelectrolyte (PE) brushes. A pressure-driven flow drives the mobile electrolyte ions of the electric double layer (EDL) supported by the charged PE brushes leading to the generation of a streaming current, a streaming electric field and eventually an electrical energy. The salient feature of this study is that the brushes are described using our recently developed augmented Strong Stretching Theory (SST) model. In all the previous theoretical studies on liquid transport in PE-brush-grafted nanochannels, the brushes have either been assumed to be of constant height (independent of salt concentration or pH) or modelled using the Alexander-de-Gennes model that considers uniform monomer distribution along the brush height. Such simplifications have meant that the salt and the pH dependence of the brush height, the monomer distribution, and the resulting electrostatics have not been appropriately accounted for in the transport calculations. This paper addresses these limitations and provides a much more detailed description of the brushes while capturing the corresponding electrokinetic energy conversion. The results establish that the presence of the PE brushes ensures a localization of the average EDL charge density away from the grafting surface, thereby enabling the migration of the EDL ions with a larger background flow velocity; as a consequence, there is an enhancement of the streaming current, streaming electric field, and the resulting electrical energy generation under certain grafting densities of the PE brushes.

I. INTRODUCTION

Functionalizing nanoscale surfaces (e.g., inner walls of a nanochannel or the surface of a nanoparticle) by grafting them with polyelectrolyte (PE) brushes that are sensitive to environmental stimuli (e.g., pH, salt concentration, etc.) has been widely employed for applications such as nanoscale sensing of ions, analytes, and biomolecules [1–5], fabrication of devices like nanofluidic diodes, current rectifiers, and nano-actuators [6–9], nanoparticle-based targeted drug delivery [10–13], oil recovery [14], water harvesting [15], emulsion stabilization [16], and many more. All these applications rely on the changes in the configurations and structures of the PE brushes in response to these environmental stimuli and the manner in which these changes affect the quantities dictated by the brushes (e.g., the ionic current, mobility of the brush-grafted nanoparticles, etc.). On the other hand, the liquid transport in PE-brush-grafted nanochannels has rarely been considered as the basis of any application. This has stemmed from the universal notion that the presence of the brushes will invariably reduce the flow in PE-brush-grafted nanochannels due to the enhanced drag imparted by the brushes [17].

A recent set of papers by Das and co-workers have led to a paradigm shift in this universal notion of reduced transport in brush-grafted nanochannels [18–21]. In these papers, the authors studied the transport of an electrolyte solution in nanochannels grafted with end-charged PE brushes containing charges at their non-grafted ends, which localized the electric double layer (EDL) at locations away from the grafting surface. Under such conditions, the effect of the body force on water resulting from the interaction of the EDL charge density with the applied electric field gets augmented, leading to an augmented electroosmotic transport in PE-brush-grafted nanochannels under certain conditions of the PE grafting density [18]. Similarly, this condition of the EDL being localized away from the nanochannel wall meant that the background velocity with which the counterions of the EDL are advected is also enhanced. This, in turn, was responsible for enhanced electrokinetic energy conversion in presence of a background pressure-driven flow [19] and enhanced diffusioosmotic [20] and thermoosmotic transport [21]. A key limitation of these papers [18–21] is that they consider a somewhat idealistic system where the charge is localized at the non-grafted end of the brushes, while the rest of the brush is uncharged and hence likely to be hydrophobic due to the alkane chain. Such a system will make the penetration of the flow within the brushes difficult, which implies that there is rarely any interaction between the brushes and the flow. These papers [18–21], however, in addition to being studies that demonstrate a positive influence of the brushes on the liquid transport, are also among the first studies that have considered a thermodynamic description of the brushes, albeit through the simplified Alexander-de-Gennes model that considers a uniform monomer distribution, in the calculation of the liquid transport in PE-brush-grafted nanochannels. In such a thermodynamic description, the brush height is quantified by the balance of the energy of a brush (consisting of the elastic, excluded volume, and the electrostatic contributions) and the electrostatic energy

of the EDL. Accordingly, these calculations are far more rigorous than a large number of previous studies, including those by the present authors, where the brush height has been assumed to be an *a priori* constant and independent of the salt concentration [17, 22–36].

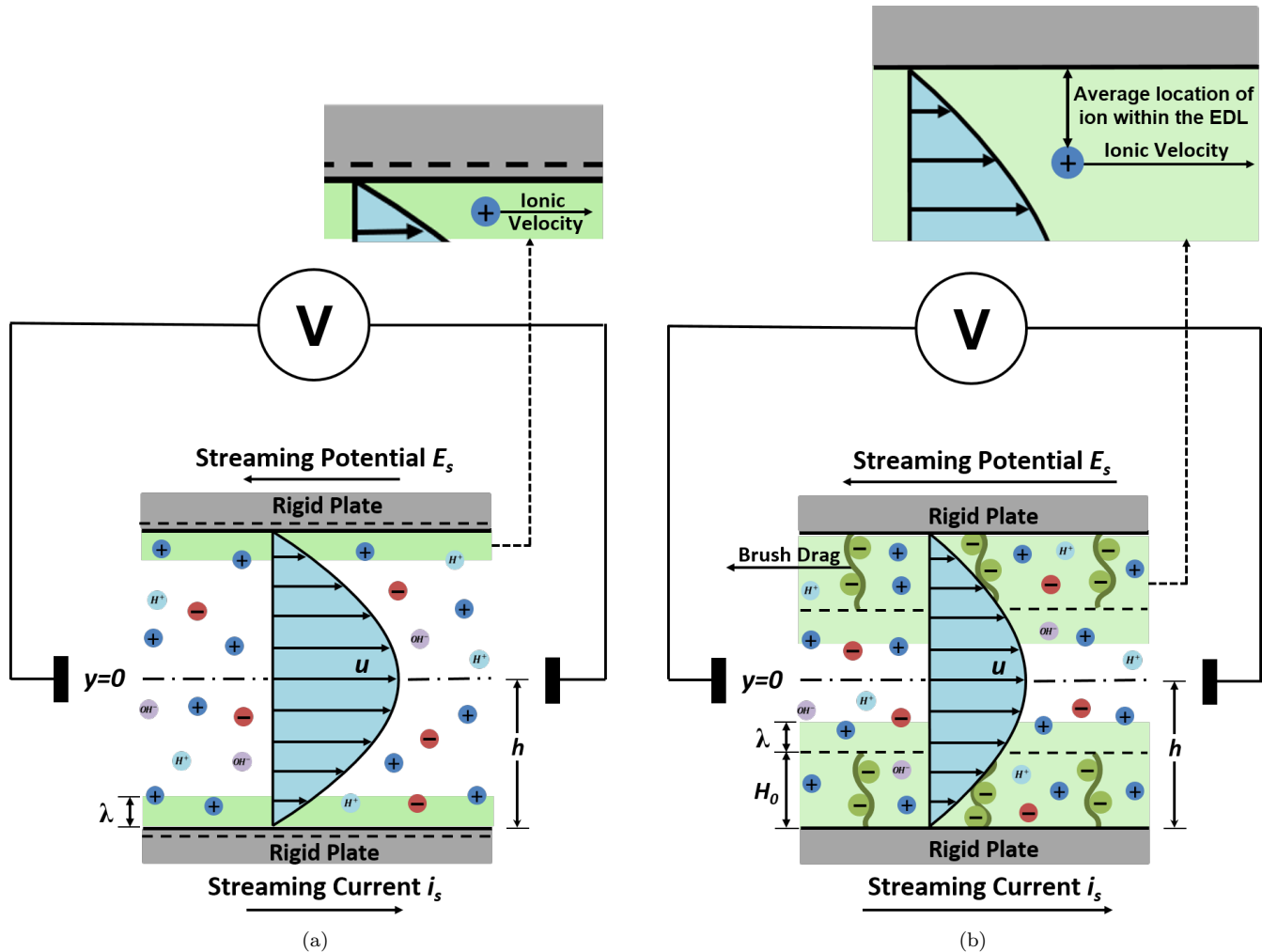


FIG. 1: Schematic depicting the generation of the streaming electric field (E_s) and streaming current (i_s) (the electrokinetically generated electric power P_{out} and the resultant energy conversion efficiency (ξ) are proportional to the product of i_s and E_s). in a) brush-free nanochannel b) backbone charged PE brushes grafted nanochannel. In the schematic, we highlight the manner in which the presence of the brushes localizes the average EDL charge density further away from the grafting surface enforcing the EDL ions to be advected by a larger background flow velocity, which in turn will lead to an enhanced i_s , E_s , P_{out} , and ξ in brush-grafted nanochannels.

In this paper, we make two major advancements over and above the calculations of the papers by Das and coworkers [18–21]. First, we consider a much more realizable and practical set up where a pressure-driven water flow is occurring in a nanochannel grafted with *backbone-charged*, pH-responsive PE brushes (i.e., the ionization of the brushes depend on the local pH). More importantly, such a configuration ensures that the entire PE brush is hydrophilic (that supports a charge and an EDL) and accordingly, will be completely wetted by the flow enforcing a flow-PE-brush interaction that might be absent for the cases of end-charged brushes [18–21]. Second, the brushes are modelled by the augmented *Strong Stretching Theory* or *SST* model. The SST model is a much more improved and complete model for describing the polymer and the PE brushes [37–40] that does not require enforcing a restrictive condition like the uniform monomer distribution along the length of the polymer brush. Very recently, the present authors provided an improvement of the SST model where the effects of the PE excluded volume interactions and an expanded form of the mass action law were considered [41]. In this paper, by employing such augmented SST for modelling the brushes, we ensure that we are developing possibly the most rigorous continuum description of liquid transport in PE-brush-grafted nanochannels till date. For the sake of completeness, we first describe the thermodynamics of the

problem, where the brush height, the monomer density and the EDL electrostatics are quantified. The EDL variation clearly points out that the presence of the brushes localize the EDL charge density away from the walls. Accordingly, in presence of the background pressure-driven transport, the presence of the brushes ensure that the average flow velocity with which the EDL ions are getting advected is much larger as compared to the brush-free nanochannels (this is illustrated in Fig. 1) leading to an enhanced streaming current and streaming electric field. As a consequence, the output power as well as the efficiency of the electrokinetic energy conversion is significantly enhanced in comparison to the brush-free nanochannels, despite the presence of the brush-induced enhanced drag. We report efficiency values of as large as 5% for brush-grafted nanochannels and establish that the efficiency improves (in comparison to the brush-free nanochannels) by several folds for both the cases of nanochannels with weakly and densely grafted pH-responsive, PE brushes. In summary, therefore, through the most rigorous theoretical description for studying electrokinetic transport in brush-grafted nanochannels till date, we establish that the functionalization by pH-responsive, charged PE brushes can significantly enhance the electrokinetic energy conversion efficiency in nanochannels.

II. THEORY

We consider a pressure driven flow in a nanochannel with half-channel height h grafted with backbone-charged, pH-responsive polyelectrolyte (PE) brushes [see Fig.1(b)]. The brushes are negatively charged, have a degree of polymerization N , a Kuhn length a , a grafting density (number of chains per unit area) of $\sigma = 1/\ell^2$ (where ℓ is the lateral space between two adjacently grafted PE brushes), and a polyelectrolyte chargeable sites (PCS) density of γ . The surrounding fluid has a dielectric constant ϵ_r , a bulk salt number density n_∞ and a bulk pH value of pH_∞ . Here the PE brushes are described by our recently developed augmented Strong Stretching Theory (SST) model [41]. Below we summarize the key equations of this model.

A. Augmented Strong Stretching Theory Model for pH-responsive PE brushes

Our augmented SST model for the PE brushes improves the existing SST models for the PE brushes [37–40] by considering the excluded volume effects and a generic value of γ (with $\gamma a^3 \neq 1$, where a is the Kuhn length). Here we summarize the key findings of this augmented SST model; for details, kindly refer to our previous paper [41]. In this theory, we first express the energy functional (F) of a given PE molecule as:

$$\frac{F}{k_B T} = \frac{F_{els}}{k_B T} + \frac{F_{EV}}{k_B T} + \frac{F_{elec}}{k_B T} + \frac{F_{EDL}}{k_B T} + \frac{F_{ion}}{k_B T}, \quad (1)$$

where F_{els} , F_{EV} , F_{elec} , F_{EDL} and F_{ion} are the elastic (entropic), excluded volume, electrostatic, electric double layer and ionization free energies (per PE molecule), respectively. For the expressions of these different energy components please refer to our previous paper [41].

We carry out a variational minimization of the above energy functional in presence of the following constraints:

$$N = \int_0^{y'} \frac{dy}{E(y, y')}, \quad (2)$$

$$N = \frac{1}{\sigma a^3} \int_0^H \phi(y) dy, \quad (3)$$

where N is the PE size (i.e., number of monomer per PE chain), $E(y, y') = dy/dn$ quantifies the local stretching of the PE chain at a distance y from the grafting surface with the end of the PE chain being located at a distance y' , $\phi(y)$ is the dimensionless monomer distribution, and H is the brush height. This minimization eventually yields the following governing equations that dictate the brush thermodynamics. These equations are:

$$n_{A^-} = \frac{K'_a \gamma}{K'_a + n_{H^+, \infty} \exp\left(-\gamma a^3 \frac{e\psi}{k_B T}\right)}, \quad (4)$$

$$\begin{aligned} \epsilon_0 \epsilon_r \left(\frac{d^2 \psi}{dy^2} \right) + e \left(n_+ - n_- + n_{H^+} - n_{OH^-} - n_{A^-} \phi \right) &= 0 & (-h \leq y \leq -h + H), \\ \epsilon_0 \epsilon_r \left(\frac{d^2 \psi}{dy^2} \right) + e \left(n_+ - n_- + n_{H^+} - n_{OH^-} \right) &= 0 & (-h + H \leq y \leq 0), \end{aligned} \quad (5)$$

$$n_{\pm} = n_{\pm,\infty} \exp\left(\mp \frac{e\psi}{k_B T}\right), \quad (6)$$

$$n_{H^+} = n_{H^+,\infty} \exp\left(-\frac{e\psi}{k_B T}\right), \quad (7)$$

$$n_{OH^-} = n_{OH^-,\infty} \exp\left(\frac{e\psi}{k_B T}\right), \quad (8)$$

$$\begin{aligned} \phi(y) = \frac{\nu}{3\omega} & \left[\left\{ 1 + \kappa^2 \left(\lambda - y^2 + \beta \frac{K'_a \gamma}{K'_a + n_{H^+,\infty} \exp\left(-\gamma a^3 \frac{e\psi}{k_B T}\right)} \right) \psi \right. \right. \\ & - \rho \left(1 - \frac{K'_a}{K'_a + n_{H^+,\infty} \exp\left(-\gamma a^3 \frac{e\psi}{k_B T}\right)} \right) \ln \left(1 - \frac{K'_a}{K'_a + n_{H^+,\infty} \exp\left(-\gamma a^3 \frac{e\psi}{k_B T}\right)} \right) \\ & - \rho \frac{K'_a}{K'_a + n_{H^+,\infty} \exp\left(-\gamma a^3 \frac{e\psi}{k_B T}\right)} \ln \left(\frac{K'_a}{K'_a + n_{H^+,\infty} \exp\left(-\gamma a^3 \frac{e\psi}{k_B T}\right)} \right) \\ & \left. \left. - \rho \frac{K'_a}{K'_a + n_{H^+,\infty} \exp\left(-\gamma a^3 \frac{e\psi}{k_B T}\right)} \ln \left(\frac{n_{H^+,\infty}}{K'_a} \right) \right\}^{1/2} - 1 \right], \quad (9) \end{aligned}$$

$$E(y, y') = \frac{\pi}{2N} \sqrt{y'^2 - y^2}, \quad (10)$$

$$(q_{net})_{H=H_0} = 0, \quad (11)$$

$$q_{net} = \frac{e}{\sigma} \int_0^h (n_+ - n_- + n_{H^+} - n_{OH^-} - \phi n_{A^-}) dy, \quad (12)$$

$$g(y) = \frac{y}{\sigma N a^3} \left[\frac{\phi(H)}{\sqrt{H^2 - y^2}} - \int_y^H \frac{d\phi(y')}{dy'} \frac{dy'}{\sqrt{y'^2 - y^2}} \right]. \quad (13)$$

Eq.(4) expresses the number density (n_{A^-}) of the A^- ion – the PE brush becomes negatively charged by producing A^- ions on their backbone via the acid-like dissociation, i.e., $HA \rightleftharpoons H^+ + A^-$. In eq.(4), $K'_a = 10^3 N_A K_a$ (where N_A is the Avogadro number and K_a is the ionization constant for the reaction $HA \rightleftharpoons H^+ + A^-$), $n_{H^+,\infty}$ is the bulk number density of the hydrogen ion concentration, $k_B T$ is the thermal energy, e is the electronic charge, and ψ is the EDL electrostatic potential. Eq.(5) is the Poisson equation expressing the distribution of the EDL electrostatic potential ψ . While expressing this equation, we consider only the bottom half of the nanochannel ($-h \leq y \leq 0$). Also, in eq.(5), ϵ_0 is the permittivity of free space, ϵ_r is the relative permittivity of the electrolyte solution (assumed identical for locations within the brushes and outside the brushes) and n_i is the number density of ion i ($i = \pm, H^+, OH^-$). Eqs.(6,7,8) provide the Boltzmann distributions expressing the ion number densities n_i in terms of the corresponding bulk number densities $n_{i,\infty}$ ($i = \pm, H^+, OH^-$). Eq.(9) expresses the monomer distribution profile. In eq.(9), ν and ω are the virial coefficients quantifying the excluded volume effects, $\kappa^2 = \frac{9\pi^2\omega}{8N^2 a^2 \nu^2}$, $\rho = \frac{8a^2 N^2}{3\pi^2}$, $\lambda = -\lambda_1 \rho = -\lambda_1 \frac{8a^2 N^2}{3\pi^2}$ [λ_1 is the Lagrange multiplier associated with the constraint expressed in eq.(3)], and $\beta = \frac{8N^2 e a^5}{3\pi^2 k_B T}$. Eq.(10) expresses the profile of the local stretching. Eq.(11) helps to obtain the equilibrium brush height H_0 . Eq.(11) is based on the net unbalanced charge q_{net} in the system, which in turn is expressed through eq.(12). Finally, eq.(13) expresses the normalized chain end distribution function that can be written as $\int_0^H g(y') dy' = 1$. The brush thermodynamics, configuration and electrostatics are obtained by solving eqs.(4-13) in a coupled fashion in presence the following boundary condition for the EDL electrostatics (assuming an uncharged grafting surface)

$$(\psi)_{y=(-h+H)^-} = (\psi)_{y=(-h+H)^+}, \quad \left(\frac{d\psi}{dy}\right)_{y=(-h+H)^-} = \left(\frac{d\psi}{dy}\right)_{y=(-h+H)^+}, \quad \left(\frac{d\psi}{dy}\right)_{y=-h} = 0, \quad \left(\frac{d\psi}{dy}\right)_{y=0} = 0. \quad (14)$$

B. Liquid Transport in PE brush Grafted Nanochannels

We apply a pressure gradient along the length of the nanochannel to drive the flow. The flow is assumed to be steady, fully developed, and one-dimensional. Due to the pressure driven flow, there is a downstream advection of the charged mobile ions present within the EDL, which in turn results in the generation of a streaming current i_s and a streaming electric field E_s . The velocity profile for the bottom half of the nanochannel (due to the pressure driven flow described above) is governed by the following incompressible, steady-state Stokes equations:

$$\begin{aligned} \eta \frac{d^2 u}{dy^2} - \frac{dp}{dx} + eE_s(n_+ - n_- + n_{H^+} - n_{OH^-}) - \frac{\eta}{\kappa_d} u &= 0 & (-h \leq y \leq -h + H_0), \\ \eta \frac{d^2 u}{dy^2} - \frac{dp}{dx} + eE_s(n_+ - n_- + n_{H^+} - n_{OH^-}) &= 0 & (-h + H_0 \leq y \leq 0). \end{aligned} \quad (15)$$

In eq.(15), h is the nanochannel half-height, u is the velocity profile, η is the dynamic viscosity of the fluid, $-\frac{dp}{dx}$ is the applied pressure gradient, E_s is the induced streaming electric field, $\kappa_d = a^2/\phi^2 = a^2\left(\frac{H_0}{\sigma a^3 N \bar{\phi}}\right)^2$, and $\bar{\phi} = \frac{\phi H_0}{\sigma a^3 N}$ [$\bar{\phi}$ is the normalized monomer distribution profile and ϕ is the monomer distribution profile expressed through eq.(9) in our augmented SST formulation]. As has been described in our previous paper [17], the term κ_d , which varies inversely as the drag coefficient (see above), can be derived from the works of de Gennes [42] and Freed and Edwards [43]. These studies [42, 43] considered the flow field within the polymer coil in a semi-dilute solution. They considered a screening length K^{-1} that screens the flow inside the polymer coil from the background flow and showed that the drag coefficient is proportional to K^2 . This case studied by de Gennes [42] and Freed and Edwards [43] resembles well with the present study, where the flow within the brushes is significantly lowered with respect to the flow outside the brushes, thereby enabling the description of the drag coefficient through an appropriate screening length K^{-1} . Under these conditions, κ_d (which varies inversely as the drag coefficient) can be expressed as $\kappa_d \sim K^{-2}$. As $K \sim \phi/a$ [44], we obtain $\kappa_d \sim a^2/\phi^2$. Finally, Eq.(15) can be expressed in non-dimensional form as:

$$\begin{aligned} \frac{d^2 \bar{u}}{d\bar{y}^2} + 1 + \frac{\bar{E}_s}{2\bar{\lambda}_D^2} [\bar{n}_{+, \infty} \exp(-\bar{\psi}) - \bar{n}_{-, \infty} \exp(\bar{\psi}) + \bar{n}_{H^+, \infty} \exp(-\bar{\psi}) - \bar{n}_{OH^-, \infty} \exp(\bar{\psi})] - \left(\frac{\sigma a^2 N \bar{\phi}}{\bar{H}_0}\right)^2 \bar{u} &= 0 & (-1 \leq \bar{y} \leq -1 + \bar{H}_0), \\ \frac{d^2 \bar{u}}{d\bar{y}^2} + 1 + \frac{\bar{E}_s}{2\bar{\lambda}_D^2} [\bar{n}_{+, \infty} \exp(-\bar{\psi}) - \bar{n}_{-, \infty} \exp(\bar{\psi}) + \bar{n}_{H^+, \infty} \exp(-\bar{\psi}) - \bar{n}_{OH^-, \infty} \exp(\bar{\psi})] &= 0 & (-1 + \bar{H}_0 \leq \bar{y} \leq 0). \end{aligned} \quad (16)$$

In eq.(16), $\bar{\psi} = \frac{e\psi}{k_B T}$, $\bar{u} = \frac{u}{u_{p,0}}$, $\bar{E}_s = \frac{E_s}{E_0}$, $\bar{n}_{i,\infty} = \frac{n_{i,\infty}}{n_\infty}$ ($i = \pm, H^+, OH^-$), $\bar{y} = \frac{y}{h}$, $\bar{H}_0 = \frac{H_0}{h}$, $\bar{\lambda}_D = \frac{\lambda_D}{h}$, where $u_{p,0} = \left(-\frac{dp}{dx}\right) \frac{h^2}{\eta}$ is the pressure-driven velocity scale, $E_0 = \frac{e\eta u_{p,0}}{\epsilon_0 \epsilon_r k_B T} = \left(-\frac{dp}{dx}\right) \frac{eh^2}{\epsilon_0 \epsilon_r k_B T}$ is the scale for the electric field and $\lambda_D = \sqrt{\epsilon_0 \epsilon_r k_B T / (2e^2 n_\infty)}$ ($n_\infty = n_{+, \infty}$) is the Debye screening length of the electric double layer (EDL) based solely on the electrolyte concentration. Of course, λ_D approaches the effective Debye screening length (due to all mobile ions) $\lambda_{D,eff} = \sqrt{\epsilon_0 \epsilon_r k_B T / [2e^2 (n_\infty + n_{H^+, \infty})]}$ for large values of pH_∞ .

The velocity field is solved under the following boundary conditions:

$$(\bar{u})_{\bar{y}=-1} = 0, \quad \left(\frac{d\bar{u}}{d\bar{y}}\right)_{\bar{y}=0} = 0, \quad (\bar{u})_{\bar{y}=(-1 + \bar{H}_0)^-} = (\bar{u})_{\bar{y}=(-1 + \bar{H}_0)^+}, \quad \left(\frac{d\bar{u}}{d\bar{y}}\right)_{\bar{y}=(-1 + \bar{H}_0)^-} = \left(\frac{d\bar{u}}{d\bar{y}}\right)_{\bar{y}=(-1 + \bar{H}_0)^+}. \quad (17)$$

The net ionic current through the nanochannel is zero since there is no applied external voltage. This leads to

$$2e \int_{-h}^0 (u_+ n_+ - u_- n_- + u_{H^+} n_{H^+} - u_{OH^-} n_{OH^-}) dy = 0, \quad (18)$$

where u_i ($i = \pm, H^+, OH^-$) are the ion migration velocities expressed as:

$$u_i = u + \frac{ez_i E_s}{f_i}. \quad (19)$$

In eq.(19), f_i is the friction coefficient (the inverse of ionic mobility) for species i ($i = \pm, H^+, OH^-$). Eq. (18) can be simplified in the presence of eqs.(6,7,8) and (19) to yield an expression for the non-dimensionalized streaming electric field as:

$$\bar{E}_s = \frac{\int_{-1}^0 \bar{u} \left[-\bar{n}_{+, \infty} \exp(-\bar{\psi}) + \bar{n}_{-, \infty} \exp(\bar{\psi}) - \bar{n}_{H^+, \infty} \exp(-\bar{\psi}) + \bar{n}_{OH^-, \infty} \exp(\bar{\psi}) \right] d\bar{y}}{\int_{-1}^0 \bar{u} \left[R_+ \bar{n}_{+, \infty} \exp(-\bar{\psi}) + R_- \bar{n}_{-, \infty} \exp(\bar{\psi}) + R_{H^+} \bar{n}_{H^+, \infty} \exp(-\bar{\psi}) + R_{OH^-} \bar{n}_{OH^-, \infty} \exp(\bar{\psi}) \right] d\bar{y}}, \quad (20)$$

where $R_i = \frac{e^2 z_i^2 \eta}{\epsilon_0 \epsilon_r k_B T f_i}$ ($i = +, -, H^+, OH^-$) is a dimensionless parameter, identified as the inverse of the ionic Peclet number. Substituting eq.(20) in eq.(16) we arrive at an integro-differential equation in \bar{u} which is solved numerically. Having obtained \bar{u} , the streaming electric field can be calculated from eq.(20). The downstream migration of mobile ions due to the flow also creates a streaming current (per unit width of the nanochannel) which can be expressed as:

$$i_s = 2e \int_{-h}^0 u(n_+ - n_- + n_{H^+} - n_{OH^-}) dy. \quad (21)$$

i_s can be calculated from the knowledge of the velocity field u . The knowledge of i_s and E_s allows us to express the net electrical power output (per unit area) as:

$$P_{out} = \left| \frac{1}{4} i_s E_s \right|. \quad (22)$$

On the other hand, the input power supplied (per unit area) to the system as a result of the applied pressure gradient is:

$$P_{in} = \left(-\frac{dp}{dx} \right) Q_{in}. \quad (23)$$

In eq.(23), Q_{in} is the volume flow rate (per unit width of the nanochannel) expressed as:

$$Q_{in} = 2 \int_{-h}^0 u_{pp} dy, \quad (24)$$

where u_{pp} is the pure pressure velocity profile accounting for flow through the PE brush grafted nanochannel without the effects of the EDL body force on the ions. u_{pp} can be obtained by solving the following ODE's:

$$\begin{aligned} \eta \frac{d^2 u_{pp}}{dy^2} - \frac{dp}{dx} - \frac{\eta}{\kappa_d} u_{pp} &= 0 & (-h \leq y \leq -h + H_0), \\ \eta \frac{d^2 u_{pp}}{dy^2} - \frac{dp}{dx} &= 0 & (-h + H_0 \leq y \leq 0), \end{aligned} \quad (25)$$

in presence of the following boundary conditions:

$$(u_{pp})_{y=-h} = 0, \quad \left(\frac{du_{pp}}{dy} \right)_{y=0} = 0, \quad (u_{pp})_{y=(-h+H_0)^-} = (u_{pp})_{y=(-h+H_0)^+}, \quad \left(\frac{du_{pp}}{dy} \right)_{y=(-h+H_0)^-} = \left(\frac{du_{pp}}{dy} \right)_{y=(-h+H_0)^+}. \quad (26)$$

Once P_{out} and P_{in} have been quantified, the corresponding electrochemomechanical energy conversion efficiency ξ can be expressed as:

$$\begin{aligned} \xi &= \frac{P_{out}}{P_{in}} \\ \Rightarrow \xi &= \frac{\left[\int_{-1}^0 \bar{u} \left[-\bar{n}_+ \exp(-\bar{\psi}) + \bar{n}_- \exp(\bar{\psi}) - \bar{n}_{H^+, \infty} \exp(-\bar{\psi}) + \bar{n}_{OH^-, \infty} \exp(\bar{\psi}) \right] d\bar{y} \right]^2}{8\bar{\lambda}^2 \int_{-1}^0 \bar{u}_{pp} d\bar{y} \int_{-1}^0 \left[\bar{n}_+ \exp(-\bar{\psi}) + \bar{n}_- \exp(\bar{\psi}) + \bar{n}_{H^+, \infty} \exp(-\bar{\psi}) + \bar{n}_{OH^-, \infty} \exp(\bar{\psi}) \right] d\bar{y}}, \end{aligned} \quad (27)$$

where $\bar{u}_{pp} = \frac{u_{pp}}{u_{p,0}}$ is the non-dimensional pure pressure-driven velocity field.

III. RESULTS AND DISCUSSIONS

We consider four different cases in this study - Case 1: Nanochannels grafted with short loose brushes ($N = 400$, $\ell = 60$ nm), Case 2: Brush-free nanochannels with an equivalent surface charge density ($\sigma_{c,eq}$) of short loose brushes (this equivalent charge density is the charge density obtained by integrating the volume charge density of the brushes along its length, i.e., $\sigma_{c,eq} = e \int_0^{H_0} \phi n_A - dy$), Case 3: Nanochannels grafted with dense brushes ($N = 400$, $\ell = 10$ nm) and Case 4: Brush-free nanochannels with an equivalent charge density of long dense brushes. The cases 1 and 2 are studied for different values of salt concentration (c_∞), pH_∞ , and γ , while the cases 3 and 4 are studied for different values c_∞ and γ for a given pH_∞ . We refrain from reporting the results for larger pH_∞ for cases 3 and 4, since for such a pH_∞ , the brush height for case 3 became much large than the chosen half height value (100 nm) of the nanochannel.

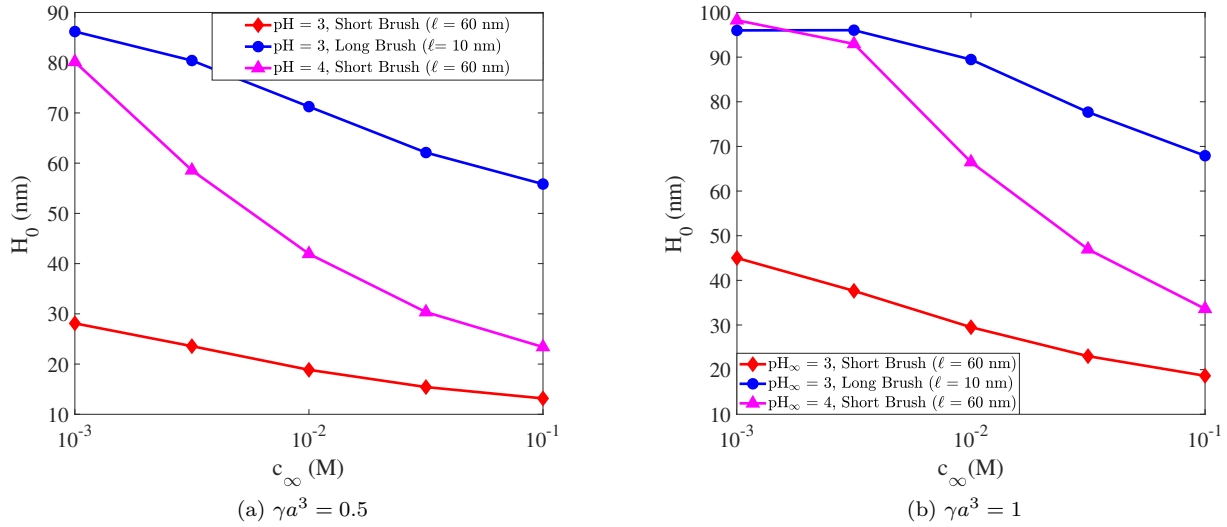


FIG. 2: Variation of equilibrium brush height H_0 with bulk salt concentration c_∞ and pH_∞ for pH-responsive, PE brush grafted nanochannels with (a) $\gamma a^3 = 0.5$ and (b) $\gamma a^3 = 1$. Here $N = 400$, $h = 100$ nm, $a = 1$ nm (Kuhn length), $k_B = 1.38 \times 10^{-23} \text{ JK}^{-1}$, $T = 298$ K, $e = 1.6 \times 10^{-19}$ C (electronic charge), $\epsilon_0 = 8.8 \times 10^{-12} \text{ Fm}^{-1}$ (permittivity of free space), $\epsilon_r = 79.8$ (relative permittivity of water), $\text{p}K_a = 3.5$, $\nu = 0.5$, $\omega = 0.1$. $\text{p}K_w = 14$, $\text{pOH}_\infty = \text{p}K_w - \text{pH}_\infty$, $c_{+, \infty} = c_\infty$, $c_{H^+, \infty} = 10^{-\text{pH}_\infty}$, $c_{OH^-, \infty} = 10^{-\text{pOH}_\infty}$, and $c_{-, \infty} = c_\infty + c_{H^+, \infty} - c_{OH^-, \infty}$.

Fig. 2 provides the variation of the brush height for the loosely grafted ($\ell = 60$ nm) and densely grafted ($\ell = 10$ nm) PE brushes as a function of the salt concentration, pH_∞ , and γ values. For a given pH_∞ and γ , an increase in the salt concentration decreases the brush height [see Figs. 2(a,b)]. A larger salt concentration leads to a smaller EDL screening length; accordingly, the brush inter-segmental repulsion gets screened over a much smaller distance enforcing a much weaker repulsion-driven stretching of the PE brushes and a much smaller value of H_0 . On the other hand, a larger pH_∞ signals a weaker bulk concentration of the H^+ ions, which will enforce a stronger ionization of the PE brushes as this ionization produces H^+ ions. Of course, a stronger ionization leads to a larger charge on the PE brush facilitating a larger inter-segmental repulsion induced enhanced value of the brush height H_0 . Finally, a larger value of γ [results are shown in Fig. 2(b)] will signify a larger charge on the brush segments and accordingly, a larger electrostatic-repulsion mediated enhanced brush height for a given value of salt concentration and pH_∞ .

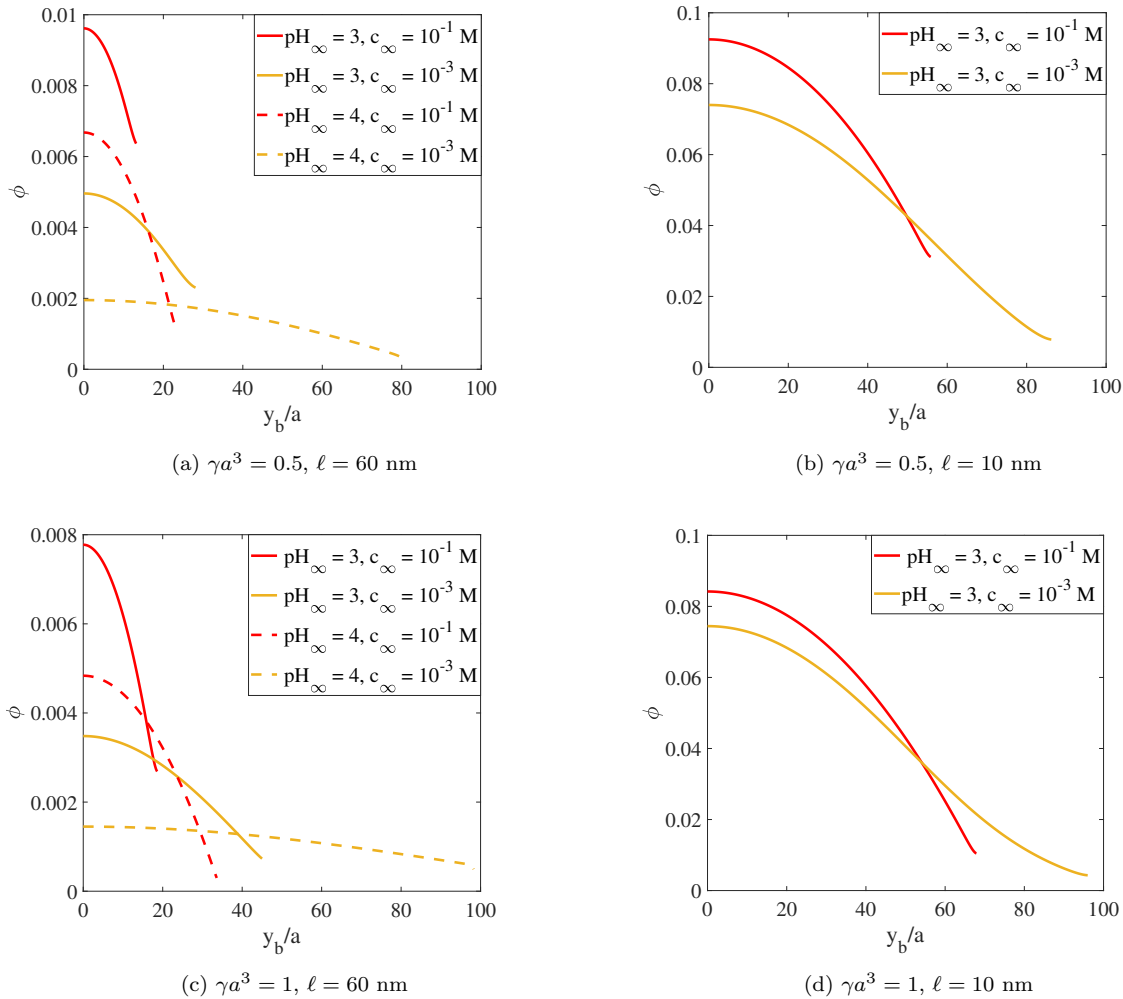


FIG. 3: Variation of monomer distribution profile ϕ with bulk salt concentration c_∞ and pH_∞ for pH-responsive, PE brush grafted nanochannels with (a) $\gamma a^3 = 0.5, \ell = 60 \text{ nm}$, (b) $\gamma a^3 = 0.5, \ell = 10 \text{ nm}$, (c) $\gamma a^3 = 1, \ell = 60 \text{ nm}$ and (d) $\gamma a^3 = 1, \ell = 10 \text{ nm}$. All the other parameters are same as those used in Fig. 2.

Fig. 3 provides the variation of the monomer distribution ϕ . Shorter brush height implies that the monomers are more densely packed near the grafting wall. Accordingly, for a given grafting density (i.e., a given value of ℓ), we find a larger value of ϕ near the wall for the cases of smaller pH_∞ (effect of the variation of pH_∞ is shown for weakly grafted brushes, i.e., $\ell = 60 \text{ nm}$) [see Figs. 3(a,c)] and larger salt concentration [see Figs. 3(a-d)]. Also, the smaller brush height for these cases (smaller pH_∞ and larger salt concentration) ensures that the ϕ profile no longer exists at larger distances away from the grafting wall. A larger grafting density σ (or smaller ℓ) ensures a larger value of ϕ at a given y since $\phi \sim \sigma$ (see eq.(3)) [compare Fig. 3(a) with Fig. 3(b) and Fig. 3(c) with Fig. 3(d)]. Finally, a larger value of γ leads to a larger brush height, which ensures, for a given pH_∞, c_∞ , and grafting density, a weaker value of the monomer density at near-wall locations and the existence of the ϕ profile over larger distances away from the wall [compare Fig. 3(a) with Fig. 3(c) and Fig. 3(b) with Fig. 3(d)].

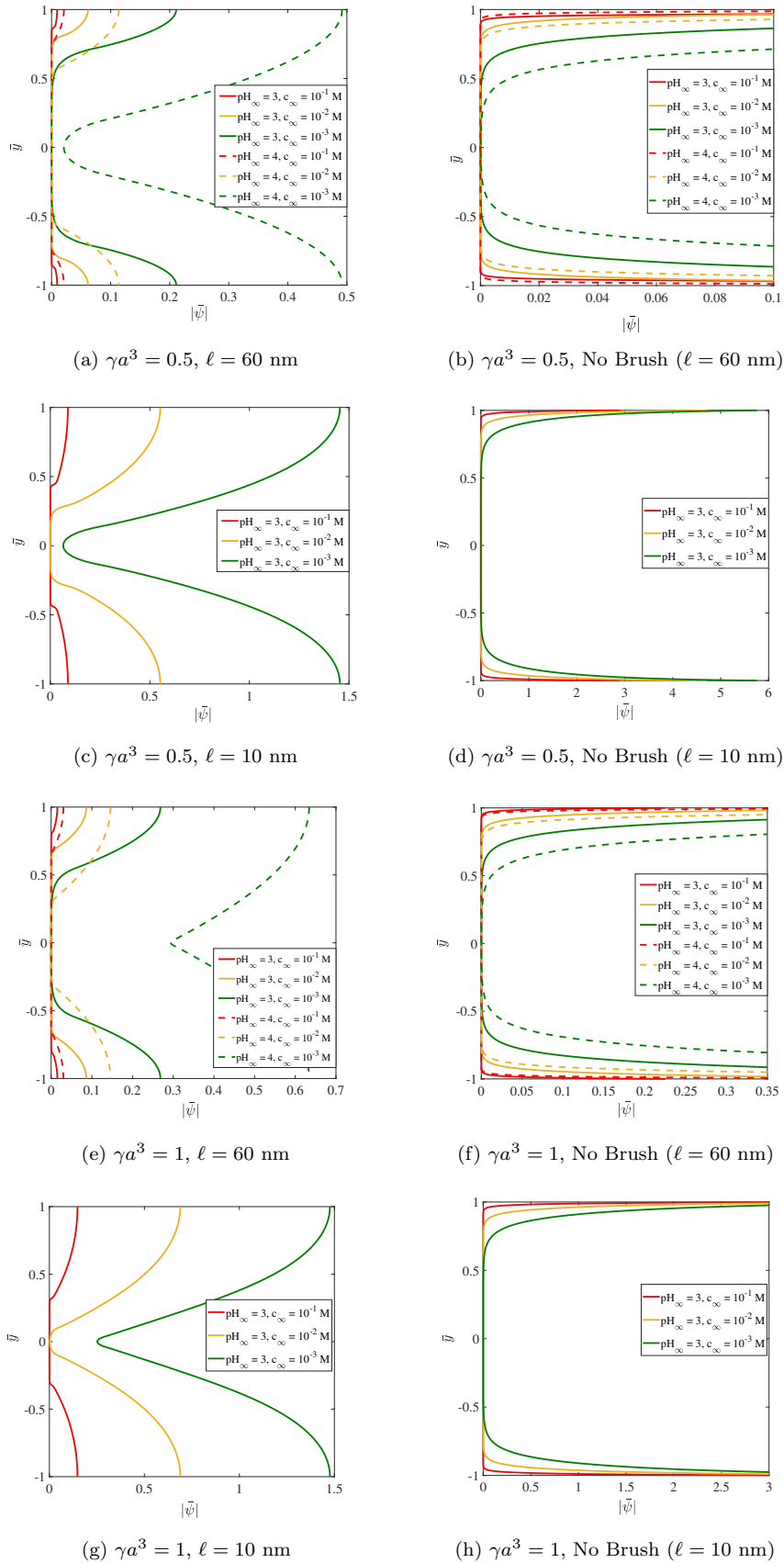


FIG. 4: Transverse variation of the non-dimensional EDL electrostatic potential $\bar{\psi}$ with bulk salt concentration c_∞ and pH_∞ for (a) PE brush-grafted nanochannel with $\gamma a^3 = 0.5, \ell = 60 \text{ nm}$, (b) brush-free nanochannel with equivalent charge density $\sigma_{c,eq}$ identical to that of the brush-grafted nanochannels with $\gamma a^3 = 0.5$ and $\ell = 60 \text{ nm}$, (c) PE brush-grafted nanochannel with $\gamma a^3 = 0.5, \ell = 10 \text{ nm}$, (d) brush-free nanochannel with equivalent charge density $\sigma_{c,eq}$ identical to that of the brush-grafted nanochannels with $\gamma a^3 = 0.5$ and $\ell = 10 \text{ nm}$, (e) PE brush-grafted nanochannel with $\gamma a^3 = 1, \ell = 60 \text{ nm}$, (f) brush-free nanochannel with equivalent charge density $\sigma_{c,eq}$ identical to that of the brush-grafted nanochannels with $\gamma a^3 = 1$ and $\ell = 60 \text{ nm}$, (g) PE brush-grafted nanochannel with $\gamma a^3 = 1, \ell = 10 \text{ nm}$ and (h) brush-free nanochannel with equivalent charge density $\sigma_{c,eq}$ identical to that of the brush-grafted nanochannels with $\gamma a^3 = 1$ and $\ell = 10 \text{ nm}$. All the parameters are

Fig. 4 provides the transverse variation of the dimensionless EDL electrostatic potential distribution ($\bar{\psi}$) within the nanochannel as a function of (i) the presence and the absence of the brushes, (ii) brushes with different grafting densities, (iii) different values of pH_∞ and c_∞ , and (iv) different values of γ . First we compare the cases of short (weak grafting density) and tall (large grafting density) brushes for a given pH_∞ , c_∞ , and γ value [i.e., we compare Fig. 4(a) with Fig. 4(c) and Fig. 4(e) with Fig. 4(g)]. For a given γ , a taller brush represents a larger charge content, which leads to a larger ψ at a given transverse location. Furthermore, a larger brush height implies that ψ exists at larger distances away from the grafting wall. For the case of a given grafting density, γ and c_∞ , a smaller pH_∞ causes a weaker charge density of the brushes leading to a weaker value of $\bar{\psi}$. Of course, this effect of the variation in pH_∞ has been portrayed for the case of weak grafting density [see Figs. 4(a,e)]. Also, an increase in c_∞ for a given grafting density, pH_∞ , and γ ensures a weaker ψ stemming from the fact that $\psi \sim \sigma_c \lambda_{D,eff}$ (where σ_c is the charge density of the PE brushes and $\lambda_{D,eff}$, which decreases with c_∞ , is the EDL thickness). Also, an increase in γ increases the charge of the PE brushes, thereby increasing $\bar{\psi}$ [compare Fig. 4(a) with Fig. 4(e) and Fig. 4(c) with Fig. 4(g)]. The most interesting comparison for ψ is between the cases of brush-free and brush-grafted nanochannels [compare Fig. 4(a) with Fig. 4(b), Fig. 4(c) with Fig. 4(d), Fig. 4(e) with Fig. 4(f), and Fig. 4(g) with Fig. 4(h)]. *For the brush-free nanochannels, the EDL electrostatic potential is entirely localized at near-wall locations – larger c_∞ leading to smaller EDL thickness leads to an even larger localization. On the other hand, the presence of the charged brushes grafted on chargeless nanochannel walls ensure that this EDL electrostatic potential gets distributed along the length of the brushes and accordingly, $\bar{\psi}$ is no longer localized at the nanochannel wall. Such a scenario obviously leads to an EDL charge density that is localized away from the wall, which in turn will massively influence the overall electrohydrodynamics (as discussed later).* Please note that in Fig. 4 as well in Figs. 5-9, the values of γ and ℓ are used for the brush-free nanochannel case as well in order to ensure that the walls of the brush-free nanochannel are an equivalent surface charge density $\sigma_{c,eq}$ of the brush-grafted nanochannels; as has been already described earlier, $\sigma_{c,eq}$ is obtained by integrating (along the brush length) the volume charge density of the PE brush, i.e., $\sigma_{c,eq} = e \int_0^{H_0} \phi n_{A-} dy$.

Fig. 5 demonstrates the velocity field in the nanochannel as a function of (i) the presence and the absence of the brushes, (ii) brushes with different grafting densities, (iii) different values of pH_∞ and c_∞ , and (iv) different values of γ . Before describing the influence of these different parameters, it is critical to identify the different components of the velocity field. Firstly, the flow is being driven by an externally imposed pressure gradient. This flow is retarded by the additional drag imparted by the brushes. Secondly, this pressure-driven flow induces a streaming electric field that triggers an electroosmotic (EOS) transport that opposes the pressure-driven transport. This retarding EOS transport itself also experiences the retarding influences of the additional drag imparted by the presence of the brushes. *However, more importantly, the streaming electric field and the streaming current are favored by the presence of the brushes stemming from the fact that the brushes localizes the average EDL charge density away from the wall (evident from the significantly large ψ values away from the wall, which is not the case for brush-free nanochannels, see Fig. 4), which ensures that the liquid velocity with which the EDL ions gets advected downstream (this downstream advection of the EDL charge density gradient induces the streaming current and the streaming electric field, see Fig. 1 for a schematic illustration) is much larger as compared to the case of the brush free nanochannel.* We first consider the effect of salt and pH_∞ for a given type of (brush-grafted or brush-free) nanochannel and a given γ . Decrease in salt concentration or an increase in pH_∞ increases ψ and therefore will increase the EDL charge density. An increase in this EDL charge density will increase the body force (which is proportional to this charge density) that drives the EOS transport. Hence the overall velocity decreases with an increase in pH_∞ and a decrease in salt concentration. Next we compare the velocity fields for the brush-free and brush-grafted (weakly grafted) nanochannels [i.e., we compare Fig. 5(a) with Fig. 5(b) and Fig. 5(e) with Fig. 5(f)]. The presence of the brushes decreases the overall velocity due to the additional drag and also due to the enhanced streaming electric field due to the EDL charge density localization away from the wall. For the case of the weakly grafted brushes, the effect of the enhanced drag is rather weak; on the other hand the effect of the enhanced streaming electric field and the consequent enhanced back EOS transport is larger. Accordingly, for cases where the streaming electric field is weak (results discussed later), i.e., for large c_∞ and small pH_∞ , we do not find a significant difference between the flow fields for the cases of brush-free and brush-grafted nanochannels. However, for the case of large pH_∞ (=4) and small c_∞ ($= 10^{-3} M$), the large streaming electric field and the resultant large retarding EOS transport significantly reduces the overall velocity. On the other hand, if we compare the cases of brush-free and brush-grafted (larger grafting density, $\ell = 10 nm$) nanochannels [i.e., we compare Fig. 5(c) with Fig. 5(d) and Fig. 5(g) with Fig. 5(h)], the enhanced brush-induced drag plays the dominant role causing a significant reduction in the velocity for the brush-grafted nanochannels. For the case of the larger γ , a larger charge of the brush leading to a larger ψ and hence a larger streaming electric field causes an even more noticeable reduction in the velocity field for the case of nanochannels with weakly grafted brushes at large pH_∞ and small c_∞ [compare Fig. 5(a) with Fig. 5(e) and Fig. 5(c) with Fig. 5(g)]. Finally, we shall like to point out the generation of negative velocities at near-wall locations for the cases of nanochannels with densely grafted brushes [cases described in Figs.

5(c), Fig. 5(g)]. As has been already pointed out, for the case of the densely grafted brushes, there is a significant reduction of the original pressure-driven velocity. This reduction is obviously most prominent at near wall locations. Consequently, the presence of a substantial induced streaming electric field (which is not a local near-wall effect and is obtained by integration across the nanochannel cross section) causing a substantial electroosmotic transport in a direction opposite to the pressure-driven flow will imply that at such near-wall locations the net local velocity becomes negative (i.e., opposite to the direction of the pressure-driven flow).

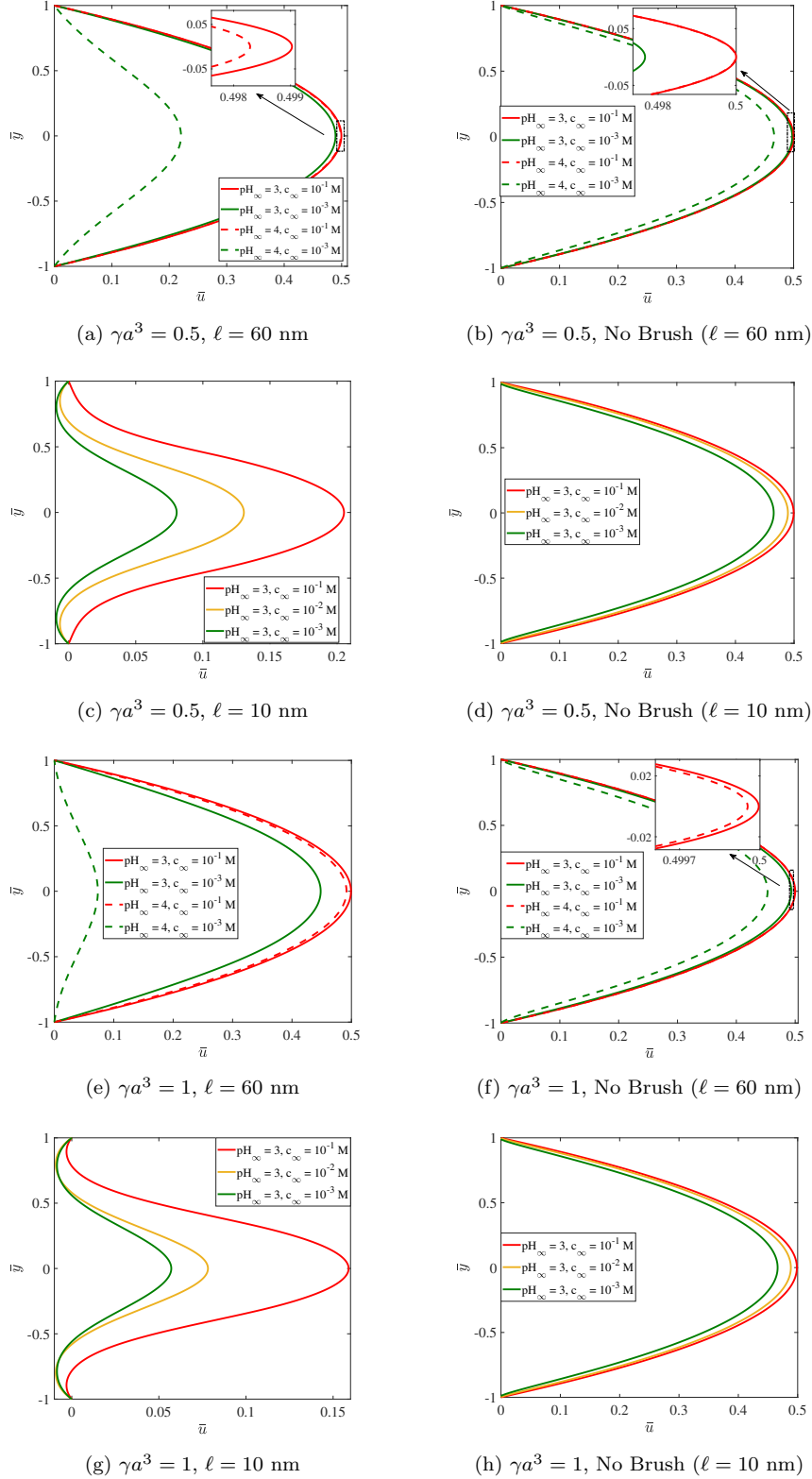


FIG. 5: Transverse variation of the non-dimensional velocity profile \bar{u} with bulk salt concentration c_∞ and pH_∞ for (a) PE brush-grafted nanochannel with $\gamma a^3 = 0.5$, $\ell = 60$ nm, (b) brush-free nanochannel with equivalent charge density $\sigma_{c,eq}$ identical to that of the brush-grafted nanochannels with $\gamma a^3 = 0.5$ and $\ell = 60$ nm, (c) PE brush-grafted nanochannel with $\gamma a^3 = 0.5$, $\ell = 10$ nm, (d) brush-free nanochannel with equivalent charge density $\sigma_{c,eq}$ identical to that of the brush-grafted nanochannels with $\gamma a^3 = 0.5$ and $\ell = 10$ nm, (e) PE brush-grafted nanochannel with $\gamma a^3 = 1$, $\ell = 60$ nm, (f) brush-free nanochannel with equivalent charge density $\sigma_{c,eq}$ identical to that of the brush-grafted nanochannels with $\gamma a^3 = 1$ and $\ell = 60$ nm, (g) PE brush-grafted nanochannel with $\gamma a^3 = 1$, $\ell = 10$ nm and (h) brush-free nanochannel with equivalent charge density $\sigma_{c,eq}$ identical to that of the brush-grafted nanochannels with $\gamma a^3 = 1$ and $\ell = 10$ nm. Here $R_i = 1$ ($i = +, -, H^+, OH^-$). All other parameters are same as those mentioned in Fig. 2.

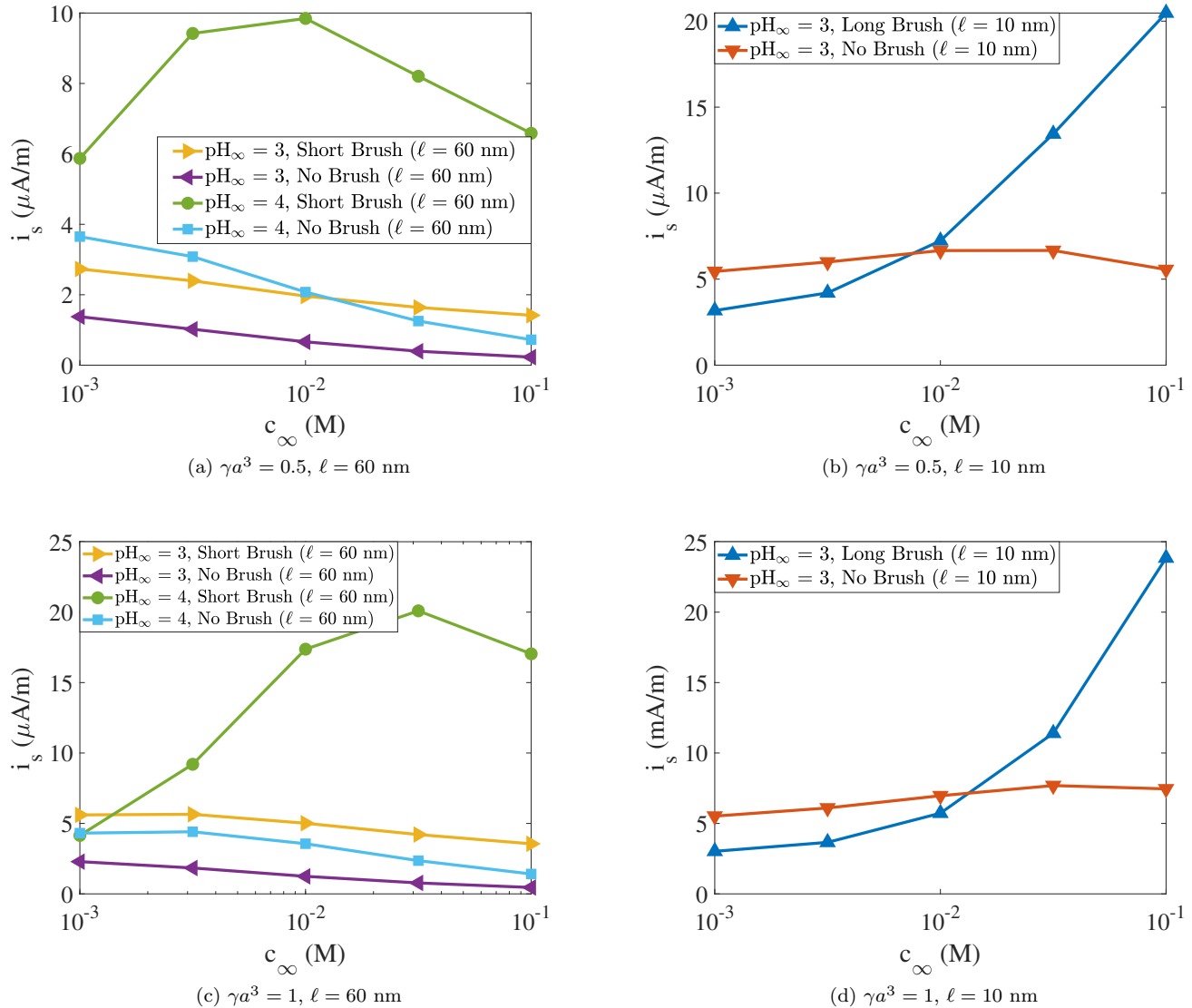


FIG. 6: Variation of streaming current i_s with bulk salt concentration c_∞ and pH_∞ for (a) brush-grafted nanochannels (with $\gamma a^3 = 0.5$, $\ell = 60$ nm) and brush-free nanochannels with equivalent charge density $\sigma_{c,eq}$ identical to that of the brush-grafted nanochannels with $\gamma a^3 = 0.5$ and $\ell = 60$ nm, (b) brush-grafted nanochannels (with $\gamma a^3 = 0.5$, $\ell = 10$ nm) and brush-free nanochannels with equivalent charge density $\sigma_{c,eq}$ identical to that of the brush-grafted nanochannels with $\gamma a^3 = 0.5$ and $\ell = 10$ nm, (c) brush-grafted nanochannels (with $\gamma a^3 = 1$, $\ell = 60$ nm) and brush-free nanochannels with equivalent charge density $\sigma_{c,eq}$ identical to that of the brush-grafted nanochannels with $\gamma a^3 = 1$ and $\ell = 60$ nm and (d) brush-grafted nanochannels (with $\gamma a^3 = 1$, $\ell = 10$ nm) and brush-free nanochannels with equivalent charge density $\sigma_{c,eq}$ identical to that of the brush-grafted nanochannels with $\gamma a^3 = 1$ and $\ell = 10$ nm. Here $\eta = 8.9 \times 10^{-4}$ Pa.s, $\frac{dp}{dx} = -5 \times 10^8$ Pa/m. All other parameters are identical to those used in Fig. 5.

We next consider the different height-averaged quantities, namely the streaming current (i_s), streaming electric field (E_s), power output (P_{out}) and the overall energy conversion efficiency (ξ). Fig. 6 provides the variation of the streaming current for the same set of parameters for which the other variables have been considered. The streaming current is induced by the downstream advection of the EDL charge density (or the EDL ions). Thus either an increase in the EDL charge density or an increase in the strength of the driving liquid flow will increase i_s . For a given nanochannel (brush-grafted or brush-free), an increase in pH_∞ or a decrease in salt concentration typically increases i_s , which can be directly attributed to a corresponding increase in ψ and hence the EDL charge density at such pH_∞ and c_∞ values. Let us now consider the case of brush-free and brush-grafted (short brushes or weakly grafted brushes) nanochannels [see Figs. 6(a,c)]. For such weak grafting densities, the brush-induced drag is not significant (as evidenced from the velocity profiles in Fig. 5). On the other hand, the effect of the brush induced localization

of the EDL charge density away from the wall, which enforces the EDL charge density (or the EDL mobile ions) to be advected by a larger non-near-wall velocity, is significant. This scenario has been pictorially explained by Fig. 1: the charge on the brush being distributed along its length, the EDL that develops in response to this charge on the brush is also distributed along the length of the brush. In comparison, for the brush-free system, all the charges are localized on the wall; accordingly the EDL that develops in response to this wall charge is also localized near the wall. Therefore, the average location of the EDL charge density is very close to the wall (or significantly away from the wall) for the case of brush-free (brush-grafted) nanochannels. The velocity profiles being very similar (as we are considering the cases of brush-free and weakly grafted brushes, see Fig. 5), this will imply that for the nanochannel with the brushes, the EDL charge density is advected with a much larger velocity (or a velocity that exists at locations away from the wall), while for the brush-free nanochannel the EDL charge density is advected with a much smaller velocity (or a velocity that exists at near-wall locations). As a result, for a given pH_∞ and c_∞ , i_s for the weakly brush-grafted nanochannel is always larger than the brush-free nanochannels. The most intriguing result is the comparison of i_s for brush-free and brush-grafted (strongly grafted) nanochannels [see Figs. 6(b,d)]. We find that for a weaker salt concentration, i_s is larger for the brush-free nanochannels, while for the larger salt concentration i_s is much larger for the brush-grafted nanochannels. At a small c_∞ , i_s is primarily dictated by the magnitude of the background flow velocity. Consequently, the extremely small (due to the combined influence of the drag from the brushes and the streaming electric field induced retarding EOS transport) value of the background velocity for the brush-grafted nanochannels ensures a weakened i_s despite the EDL charge localization away from the nanochannel wall. On the other hand, the significant increase in the background velocity with an increase in the salt concentration for the case of nanochannels with densely grafted brushes (see Fig. 5) ensures that the effect of localization of the charge density away from the nanochannel wall becomes severely strong. Accordingly, at a large salt concentration i_s is much larger for the nanochannels with densely grafted brushes in comparison to the brush-free nanochannels. In fact, this also explains why i_s for the nanochannels with densely grafted brushes shows a massive increase with an increase in c_∞ . Interestingly, the large increase in the velocity with an increase in salt concentration (from $10^{-3} M$ to $10^{-2} M$) at a large pH_∞ ($=4$) for nanochannels with weakly grafted brushes [see Figs. 5(a,e)] gets reflected as a corresponding increase in i_s for nanochannels with weakly grafted brushes at this pH_∞ and salt concentrations [see Figs. 6(a,c)]. However, as the salt concentration is increased further, velocity increases much less so that the effect of reduced ψ and charge density becomes important leading to a decrease in i_s . This explains the highly non-intuitive and non monotonic variation of i_s with c_∞ for nanochannels with weakly grafted brushes at this $\text{pH}_\infty = 4$. Very similar trends are noted for the case of larger γ [compare Fig. 6(a) with Fig. 6(c) and Fig. 6(b) with Fig. 6(d)], although for larger γ for most of the cases, i_s is larger due to a larger charge density of the brushes that lead to a larger ψ and a larger EDL charge density. From these figures, we can also compare the i_s values for the cases of nanochannels with densely and weakly grafted brushes. The densely grafted brushes always impart a larger drag ensuring a weakened velocity in comparison to the case of nanochannels with weakly grafted brushes for all values of c_∞ and pH (see Fig. 5). On the other hand, the magnitude of the electrostatic potential and hence the EDL charge density is larger for the case of densely grafted brushes in comparison to the case of nanochannels with weakly grafted brushes for all values of c_∞ and pH (see Fig. 4). For weaker salt concentrations ($c_\infty \sim 10^{-3} M$), the extent of the velocity reduction for the nanochannels with densely grafted brushes is much larger (see Fig. 5). Accordingly, for such concentrations, i_s for the case of the nanochannels with densely grafted brushes is smaller or comparable to that of the nanochannels with weakly grafted brushes. However, the velocity reduction for the case of densely grafted brushes is much lesser for larger salt concentrations ($c_\infty \sim 10^{-1} M$). Accordingly, at such concentrations, the impact of the larger EDL charge density for the case of nanochannels with densely grafted brushes becomes critical ensuring an i_s value that is significantly larger for the case of the densely grafted brushes as compared to the case of weakly grafted brushes [compare Fig. 6(a) with Fig. 6(b) and Fig. 6(c) with Fig. 6(d)].

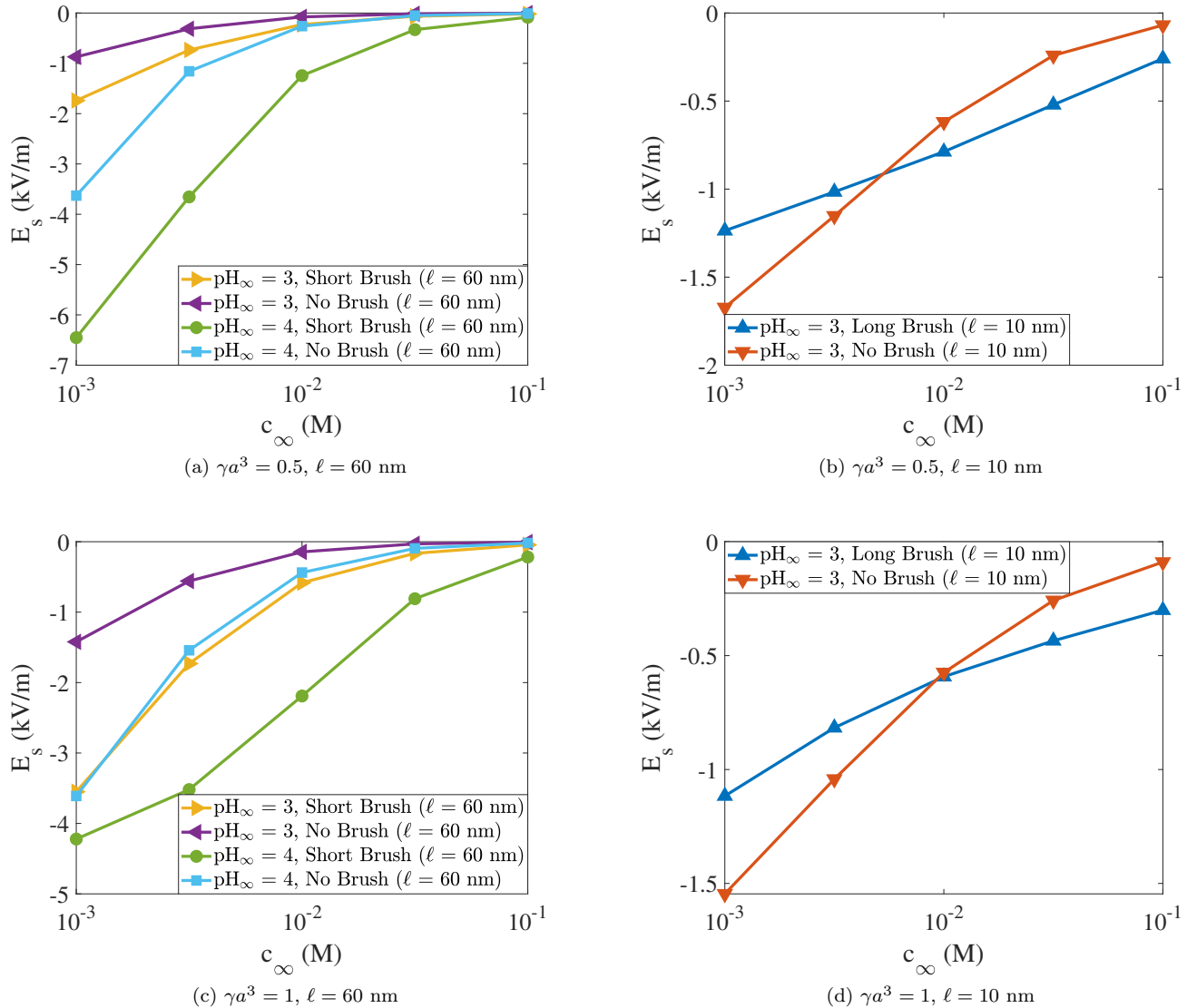


FIG. 7: Variation of streaming electric field E_s with bulk salt concentration c_∞ and pH_∞ for (a) brush-grafted nanochannels (with $\gamma a^3 = 0.5, \ell = 60$ nm) and brush-free nanochannels with equivalent charge density $\sigma_{c,eq}$ identical to that of the brush-grafted nanochannels with $\gamma a^3 = 0.5$ and $\ell = 60$ nm, (b) brush-grafted nanochannels (with $\gamma a^3 = 0.5, \ell = 10$ nm) and brush-free nanochannels with equivalent charge density $\sigma_{c,eq}$ identical to that of the brush-grafted nanochannels with $\gamma a^3 = 0.5$ and $\ell = 10$ nm, (c) brush-grafted nanochannels (with $\gamma a^3 = 1, \ell = 60$ nm) and brush-free nanochannels with equivalent charge density $\sigma_{c,eq}$ identical to that of the brush-grafted nanochannels with $\gamma a^3 = 1$ and $\ell = 60$ nm and (d) brush-grafted nanochannels (with $\gamma a^3 = 1, \ell = 10$ nm) and brush-free nanochannels with equivalent charge density $\sigma_{c,eq}$ identical to that of the brush-grafted nanochannels with $\gamma a^3 = 1$ and $\ell = 10$ nm. All other parameters are identical to those used in Fig. 6.

Fig. 7 shows the variation of the streaming electric field E_s , which can be related to i_s as $E_s \propto i_s/\Gamma$ [19] where Γ is the ionic conductivity that is proportional to the sum of the local concentration of the ions. Accordingly, the variation of E_s with the different parameters show mostly a similar trend as the corresponding variation of i_s , except for the variation with c_∞ . As $\Gamma \sim c_\infty$, i.e., $E_s \sim 1/c_\infty$ (for a given i_s), E_s invariably decreases monotonically with an increase in c_∞ . This is in contrast to the variation of i_s , which does not show a definite trend with respect to c_∞ (see Fig. 6). On the other hand, when we compare E_s for the cases of brush-free and brush-grafted (weakly grafted) nanochannels [see Figs. 7(a,c)], we invariably find that for a given value of c_∞ and pH_∞ , E_s for the brush-grafted nanochannels is significantly more than that of the brush-free nanochannels. This behavior stems directly from the corresponding variation of i_s . As $\Gamma \sim c_\infty$, i.e., $E_s \sim 1/c_\infty$ (for a given i_s), this difference in E_s between the cases of brush-free and brush-grafted nanochannels gets much more magnified at smaller c_∞ . We next compare the cases of brush-free and brush-grafted (strongly grafted) nanochannels [see Figs. 7(b,d)]. Very much like the variation of

i_s , here too we find that E_s is smaller (larger) for the brush-grafted nanochannels in comparison to the brush-free nanochannels for smaller (larger) c_∞ values. An interesting observation here is that, unlike the comparison between the brush-free and brush-grafted (weakly grafted) nanochannels, the streaming potential is not significantly large at small c_∞ despite the fact that $E_s \sim 1/c_\infty$ (for a given i_s). For the present case of brush-free and brush-grafted (strongly grafted) nanochannels, the magnitude of $\bar{\psi}$ is much higher leading to a much larger values of counterion concentration (c_+ or equivalently n_+) for a given value of c_∞ . This ensures that $\Gamma \sim c_\infty \exp(-\bar{\psi})$ is not lowered significantly even at small c_∞ and hence E_s is not massively enhanced. Finally, in Fig. 7c and 7d we study the effect of increasing γ on E_s . Increase in γ increases i_s , but at the same time also increases ψ that leads to an increase in Γ . Therefore, the change in E_s with this increase in Γ is dictated by this competitive interplay of an increase in i_s and Γ . Accordingly, for some parameter combination E_s increases with γ , while for other it decreases with an increase in γ . Of course, the overall trend with respect to other variables (i.e., c_∞ , pH_∞ , presence or absence of the brushes, grafting density of the brushes, etc.) remain unchanged with an increase in γ . Fig. 7 is a key finding of this paper. Streaming electric field (E_s) has been considered as a key measure of induced electrokinetic effects in charged nanochannels. *Fig. 7 establishes that the presence of the brushes can significantly enhance E_s by localizing the EDL charge density away from the nanochannel walls and this enhancement can be witnessed across a wide range of salt concentration, pH, and grafting density values.* From these figures, we can also compare the E_s values for the cases of nanochannels with densely and weakly grafted brushes. Variation of E_s directly follows the trends of i_s . Therefore, for smaller (larger) salt concentrations, namely $c_\infty \sim 10^{-3} M$ ($c_\infty \sim 10^{-1} M$), E_s for the nanochannels with densely grafted brushes is smaller (larger) that that for nanochannels with weakly grafted brushes [compare Fig. 7(a) with Fig. 7(b) and Fig. 7(c) with Fig. 7(d)].

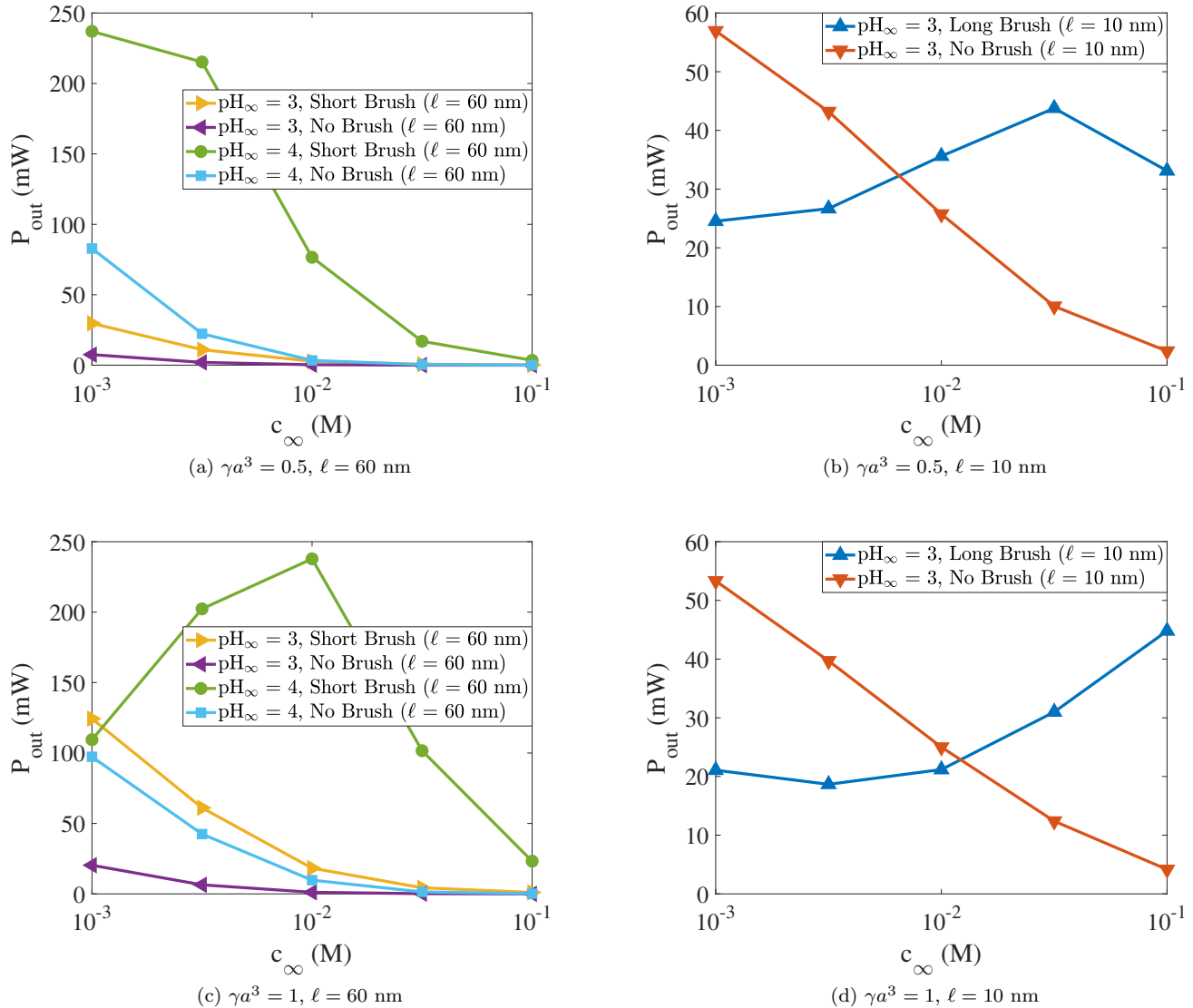


FIG. 8: Variation of net power output P_{out} with bulk salt concentration c_{∞} and pH_{∞} for (a) brush-grafted nanochannels (with $\gamma a^3 = 0.5$, $\ell = 60$ nm) and brush-free nanochannels with equivalent charge density $\sigma_{c,eq}$ identical to that of the brush-grafted nanochannels with $\gamma a^3 = 0.5$ and $\ell = 60$ nm, (b) brush-grafted nanochannels (with $\gamma a^3 = 0.5$, $\ell = 10$ nm) and brush-free nanochannels with equivalent charge density $\sigma_{c,eq}$ identical to that of the brush-grafted nanochannels with $\gamma a^3 = 0.5$ and $\ell = 10$ nm, (c) brush-grafted nanochannels (with $\gamma a^3 = 1$, $\ell = 60$ nm) and brush-free nanochannels with equivalent charge density $\sigma_{c,eq}$ identical to that of the brush-grafted nanochannels with $\gamma a^3 = 1$ and $\ell = 60$ nm and (d) brush-grafted nanochannels (with $\gamma a^3 = 1$, $\ell = 10$ nm) and brush-free nanochannels with equivalent charge density $\sigma_{c,eq}$ identical to that of the brush-grafted nanochannels with $\gamma a^3 = 1$ and $\ell = 10$ nm. A microchip (with dimensions of 1mm x 10cm x 10cm and a porosity of 0.5) containing multiple nanochannels of half-height $h = 100$ nm is considered for the calculation of output power [19]. All other parameters are identical to those used in Fig. 6.

Fig. 8 shows the variation of the electrokinetically induced output electrical power P_{out} which is proportional to the product of i_s and E_s . Accordingly, P_{out} is invariably larger for the brush-grafted (weakly grafted) nanochannels as compared to the brush-free nanochannels for any given value of c_{∞} and pH_{∞} [see Figs. 8(a,c)], since both i_s and E_s are larger for these parameters for the brush-grafted (weakly grafted) nanochannel. On the other hand, P_{out} is smaller (larger) for brush-grafted (strongly grafted) nanochannel as compared to brush-free nanochannels for smaller (larger) salt concentration, stemming from the exact similar variation for i_s and E_s . The variation of P_{out} with c_{∞} for a given type of nanochannel (brush-free or brush-grafted) for a given pH_{∞} and γ becomes interesting since it depends on the relative variation of i_s and E_s with c_{∞} . Except for the case of nanochannels with densely grafted brushes and nanochannels with weakly grafted brushes for large pH_{∞} and large γ , the decrease in E_s and i_s (typically) with c_{∞}

ensures a decrease in P_{out} with c_∞ . For the nanochannels with densely grafted brushes, different trends are observed for different values of γ . For larger (smaller) γ , the significant increase (decrease) in i_s (E_s) becomes the dominant factor at large c_∞ leading to an increase (decrease) in P_{out} for c_∞ ranging from $10^{-2} M$ to $10^{-1} M$ [see Figs. 8(b,d)]. Finally, for nanochannels with weakly grafted brushes and large pH_∞ and large γ , the dominant role of i_s for small c_∞ values ensures that P_{out} increases with c_∞ for c_∞ ranging from $10^{-3} M$ to $10^{-2} M$, while the overwhelming influence of E_s for large c_∞ values ensure a decrease in P_{out} with c_∞ for c_∞ ranging from $10^{-2} M$ to $10^{-1} M$ [see Figs. 8(a,c)]. From these figures, we can also compare the P_{out} values for the cases of nanochannels with densely and weakly grafted brushes. P_{out} is proportional to the product of i_s and E_s . Therefore, P_{out} follows the same trend as that followed by both i_s and E_s ; hence for smaller (larger) salt concentrations, namely $c_\infty \sim 10^{-3} M$ ($c_\infty \sim 10^{-1} M$), P_{out} for the nanochannels with densely grafted brushes is smaller (larger) than that for the nanochannels with weakly grafted brushes [compare Fig. 8(a) with Fig. 8(b) and Fig. 8(c) with Fig. 8(d)].

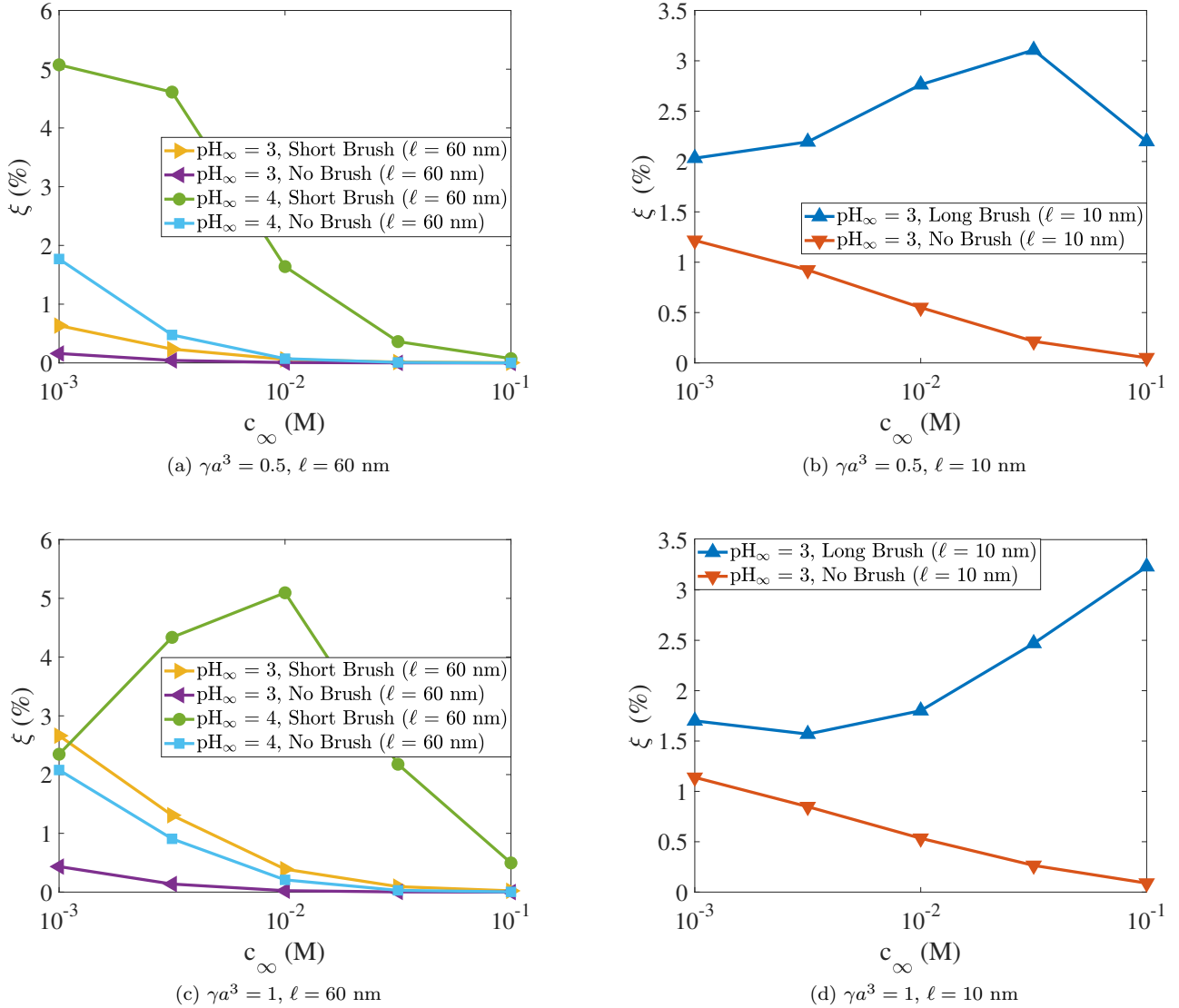


FIG. 9: Variation of electrokinetic energy efficiency ξ with bulk salt concentration c_∞ and pH_∞ for (a) brush-grafted nanochannels (with $\gamma a^3 = 0.5$, $\ell = 60$ nm) and brush-free nanochannels with equivalent charge density $\sigma_{c,eq}$ identical to that of the brush-grafted nanochannels with $\gamma a^3 = 0.5$ and $\ell = 60$ nm, (b) brush-grafted nanochannels (with $\gamma a^3 = 0.5$, $\ell = 10$ nm) and brush-free nanochannels with equivalent charge density $\sigma_{c,eq}$ identical to that of the brush-grafted nanochannels with $\gamma a^3 = 0.5$ and $\ell = 10$ nm, (c) brush-grafted nanochannels (with $\gamma a^3 = 1$, $\ell = 60$ nm) and brush-free nanochannels with equivalent charge density $\sigma_{c,eq}$ identical to that of the brush-grafted nanochannels with $\gamma a^3 = 1$ and $\ell = 60$ nm and (d) brush-grafted nanochannels (with $\gamma a^3 = 1$, $\ell = 10$ nm) and brush-free nanochannels with equivalent charge density $\sigma_{c,eq}$ identical to that of the brush-grafted nanochannels with $\gamma a^3 = 1$ and $\ell = 10$ nm. All other parameters are identical to those used in Fig. 6.

Finally, Fig. 9 shows the variation of the efficiency (ξ) of the electrokinetic energy conversion, which refers to this generation of the electrical energy from a combined mechanical energy (associated with the pressure driven flow) and chemical energy (associated with the EDL). ξ is proportional to P_{out} . Therefore, ξ is much larger for the brush-grafted nanochannels (weakly grafted) as compared to the brush-free nanochannels for any given value of pH_∞ , c_∞ , and γ [see Figs. 9(a,c)]. Also, for small γ , the nanochannel with weakly grafted brushes demonstrate a monotonic decrease in ξ with c_∞ for all pH_∞ . However, for larger γ at a large pH_∞ , ξ , very much like P_{out} is non-monotonic with c_∞ for nanochannels with weakly-grafted PE brushes [see Fig. 9(c)]. A much more interesting situation arises when we compare the cases of brush-free nanochannels and brush-grafted (densely grafted) nanochannels [see Figs. 9(b,d)]. Here too ξ for the brush-grafted nanochannels is always larger than the brush-free nanochannels (i.e., for any given value of c_∞ and γ), despite the fact that P_{out} for the brush-grafted nanochannels is smaller than the brush-free nanochannels for small c_∞ . This deviation in the trend between P_{out} and ξ for small c_∞ stems from the fact that $\xi = P_{out}/P_{in}$ and P_{in} is significantly reduced in presence of the densely-grafted brushes enforcing an enhancement of ξ even for the situation where P_{out} is reduced. It is also worthwhile to note that for nanochannels with weakly grafted brushes for relatively small c_∞ ($\sim 10^{-3} M$), large pH_∞ and small γ , we get an extremely large conversion efficiency of 5%, which is several times larger than that obtained for the corresponding brush-free nanochannels [see Fig. 9(a)]. On the other hand for a larger γ , similar efficiency (5%) is obtained at an intermediate c_∞ ($\sim 10^{-2} M$) for large pH_∞ for nanochannels with weakly grafted brushes [see Fig. 9(c)]. For the densely grafted brushes, the efficiency numbers are slightly smaller ($\sim 3\%$), although they are always larger than the corresponding brush-free nanochannels and also they are witnessed for intermediate c_∞ ($\sim 10^{-2} M$) and large c_∞ ($\sim 10^{-1} M$) values for small and large γ values [see Figs. 9(b,d)]. From these figures, we can also compare the ξ values for the cases of nanochannels with densely and weakly grafted brushes. ξ is proportional to P_{out} ; therefore following the same trend as P_{out} , at larger salt concentration ($c_\infty \sim 10^{-1} M$), ξ is larger for the case of nanochannels with densely grafted brushes. However, ξ also depends inversely on the input power P_{in} . The presence of the densely grafted brushes severely reduces P_{in} . As a consequence, only for $\gamma a^3 = 1$, at smaller salt concentration ($c_\infty \sim 10^{-3} M$), ξ is smaller for the case of nanochannels with densely grafted brushes, while for $\gamma a^3 = 0.5$ at the same small salt concentration ($c_\infty \sim 10^{-3} M$), the effect of the reduced P_{in} becomes significant ensuring a larger ξ even for the case of nanochannels with densely grafted brushes. Finally, it is worthwhile to mention here that while there has been no experiments on electrokinetic energy conversion in nanochannels grafted with PE brushes, some previous experimental studies on electrokinetic energy conversion in non-functionalized charged-wall nanochannels have reported such efficiency (3-5%) values [45-47].

IV. CONCLUSIONS

In this paper, we describe the electrokinetic energy generation in a nanochannel grafted with pH-responsive PE brushes by modelling the PE brushes with our recently developed augmented SST model. Such advanced theoretical description of the PE brushes ensures that to the best of our knowledge this is the most advanced and rigorous description of electrokinetic transport in PE-brush-grafted nanochannels. Our results establish that the brushes localize the EDL charge density away from the nanochannel wall, enforcing the advection of this charge density or the EDL ions with a much large background liquid velocity. This advection is responsible for the generation of the streaming current and the streaming electric field. As a consequence, depending on salt concentration, pH, γ , and the grafting density of the brushes, there is a significant enhancement of the streaming current and streaming electric field. In fact, this enhancement is so pronounced that it leads to an energy conversion efficiency as large as 5% for a wide combination of system parameters and more importantly, this energy conversion for nanochannels functionalized with both weakly-grafted and strongly grafted brushes can be several times larger than the corresponding brush-free nanochannels. In summary, the present paper through an extremely rigorous and complete theoretical model shows the utility of functionalizing nanochannels with PE brushes for highly efficient electrokinetic energy conversion.

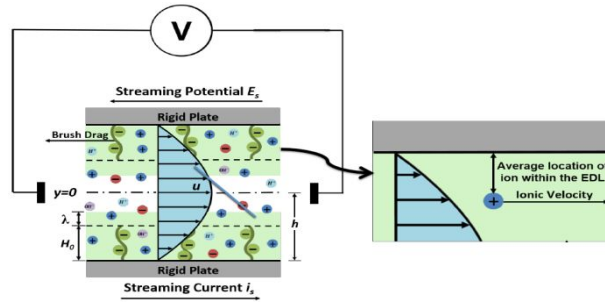
Acknowledgement: This work has been supported by the Department of Energy Office of Science grant DE-SC0017741.

References

- [1] G. W. de Groot, M. G. Santonicola, K. Sugihara, T. Zambelli, E. Reimhult, J. Voros and G. J. Vancso, *ACS Appl. Mater. Interface.*, 2013, **5**, 1400.
- [2] B. Yameen, M. Ali, R. Neumann, W. Ensinger, W. Knoll and O. Azzaroni, *J. Am. Chem. Soc.*, 2009, **131**, 2070.

- [3] M. Ali, B. Yameen, R. Neumann, W. Ensinger, W. Knoll and O. Azzaroni, *J. Am. Chem. Soc.*, 2008, **130**, 16351.
- [4] M. Ali, B. Schiedt, R. Neumann and W. Ensinger, *Macromol. Biosci.*, 2010, **10**, 28.
- [5] S. Umehara, M. Karhanek, R. W. Davis and N. Pourmand, *Proc. Natl. Acad. Sci.*, 2009, **106**, 4611.
- [6] B. Vilozny, A. L. Wollenberg, P. Actis, D. Hwang, B. Singaram, and N. Pourmand, *Nanoscale* 2013, **5**, 9214.
- [7] M. Ali, P. Ramirez, S. Mafe, R. Neumann and W. Ensinger, *ACS Nano*, 2009, **3**, 603.
- [8] M. Ali, B. Yameen, J. Cervera, P. Ramirez, R. Neumann, W. Ensinger, W. Knoll, O. Azzaroni, *J. Am. Chem. Soc.* 2010, **132**, 8338.
- [9] S. Moya, O. Azzaroni, T. Farhan, V. L. Osborne, W. T. S. Huck, *Angewand. Chem. Int. Ed.*, 2005, **44**, 4578.
- [10] S. Mura, J. Nicolas, and P. Couvreur, *Nature Mater.*, 2013, **12**, 991.
- [11] P. Colombo, F. Sonvico, G. Colombo and R. Bettini, *Pharm. Res.*, 2009, **26**, 601.
- [12] E. Gullotti and Y. Yeo, *Mol. Pharmaceutics*, 2009, **6**, 1041.
- [13] C. H. J. Choi, J. E. Zuckerman, P. Webster and M. E. Davis, *Proc. Natl. Acad. Sci. U.S.A.*, 2011, **108**, 6656.
- [14] H. ShamsiJazeyi, C. A. Miller, J. S. Wong, J. M. Tour and R. Verduzco, *J. Appl. Pol. Sci.*, 2014, **131**, 40576.
- [15] G. Liu, M. Cai, X. Wang, F. Zhou and W. Liu, *ACS Appl. Mater. Interfaces*, 2014, **6**, 11625.
- [16] N. Saleh, T. Sarbu, K. Sirk, G. V. Lowry, K. Matyjaszewski and R. D. Tilton, *Langmuir* 2005, **21**, 9873.
- [17] G. Chen and S. Das, *J. Appl. Phys.*, 2015, **117**, 185304.
- [18] G. Chen and S. Das, *J. Phys. Chem. B*, 2017, **121**, 3130.
- [19] G. Chen, H. S. Sachar, and S. Das, *Soft Matt.*, 2018, **14**, 5246.
- [20] R. S. Maheedhara, H. S. Sachar, H. Jing and S. Das, *J. Phys. Chem. B*, 2018, **122**, 7450.
- [21] R. S. Maheedhara, H. Jing, H. S. Sachar and S. Das, *Phys. Chem. Chem. Phys.*, 2018, **20**, 24300.
- [22] S. Chanda, S. Sinha and S. Das, *Soft Matt.*, 2014, **10**, 7558.
- [23] G. Chen and S. Das, *J. Colloid Interface Sci.*, 2015, **445**, 357.
- [24] J. Patwary, G. Chen and S. Das, *Microfluid. Nanofluid.*, 2016, **20**, 37.
- [25] A. Poddar, D. Maity, A. Bandopadhyay and S. Chakraborty, *Soft Matt.*, 2016, **12**, 5968.
- [26] Y. Jian, F. Li, Y. Liu, L. Chang, Q. Liu and L. Yang, *Colloid. Surf. B*, 2017, **156**, 405.
- [27] Z. Milne, L. H. Yeh, T. H. Chou and S. Qian, *J. Phys. Chem. C*, 2015, **118**, 19806.
- [28] L.-H. Yeh, M. Zhang, N. Hu, S. W. Joo, S. Qian and J.-P. Hsu, *Nanoscale*, 2012, **4**, 5169.
- [29] L.-H. Yeh, M. Zhang, N. Hu, S. W. Joo, S. Qian and J.-P. Hsu, *Anal. Chem.*, 2012, **84**, 9615.
- [30] L. Benson, L.-H. Yeh, T.-H. Chou and S. Qian, *Soft Matt.*, 2013, **9**, 9767.
- [31] C. Zhou, L. Mei, Y.-S. Su, L.-H. Yeh, X. Zhang and S. Qian, *Sens. Actuators B*, 2016, **229**, 305.
- [32] F. Li, Y. Jian, L. Chang, G. Zhao and L. Yang, *Colloid. Surf. B*, 2016, **147**, 234.
- [33] Q. Cao and H. You, *Polymers*, 2016, **8**, 438.
- [34] F. Li, Y. Jian, Z. Xie, Y. Liu and Q. Liu, *RSC Adv.*, 2017, **7**, 782.
- [35] G. Chen, J. Patwary, H. S. Sachar and S. Das, *Microfluid. Nanofluid.*, 2018, **22**, 112.
- [36] J.-S. Sin and U.-H. Kim, *Phys. Chem. Chem. Phys.*, 2018, **20**, 22961.
- [37] E. B. Zhulina, O. V. Borisov, *J. Chem. Phys.*, 1997, **107**, 5952.
- [38] Y. V. Lyatskaya, F. A. M. Leermakers, G. J. Fleer, E. B. Zhulina and T. M. Birshtein, *Macromolecules*, 1995, **28**, 3562.
- [39] I. O. Lebedeva, E. B. Zhulina and O. V. Borisov, *J. Chem. Phys.*, 2017, **146**, 214901.
- [40] E. B. Zhulina, J. K. Wolterink and O. V. Borisov, *Macromolecules*, 2000, **33**, 4945.
- [41] H. S. Sachar, V. S. Sivasankar and S. Das, *Soft Matt.*, 2019, **15**, 559.
- [42] P. G. de Gennes, *Macromolecules*, 1976, **9**, 594.
- [43] K. F. Freed and S. F. Edwards, *J. Chem. Phys.*, 1974, **61**, 3626.
- [44] J. Klein, *Colloid. Surf. A*, 1994, **61**, 3626.
- [45] H. Daiguji, P. Yang, A. J. Szeri, and A. Majumdar, *Nano Lett.*, 2004, **4**, 2315.
- [46] F. H. van der Heyden, D. Stein, and C. Dekker, *Phys. Rev. Lett.*, 2005, **95**, 116104.
- [47] F. H. van der Heyden, D. J. Bonthuis, D. Stein, C. Meyer, and C. Dekker, *Nano Lett.*, 2006, **6**, 2232.

TOC ENTRY



Augmented Strong Stretching Theory Has Been Employed to Establish that Functionalization of Nanochannels with Polyelectrolyte Brushes Enhances Electrokinetic Energy Conversion